Hindawi
Shock and Vibration
Volume 2021, Article ID 7937459, 10 pages
https://doi.org/10.1155/2021/7937459

Research Article

Study on Dynamic Behavior and Energy Dissipation of Rock considering Initial Damage Effect

Aihong Lu,[1] **Jinhai Xu**,[2] **Yu Xia**,[1] **and Lei Sun**[2]

[1]*School of Mechanics and Civil Engineering, China University of Mining and Technology, Xuzhou 221116, Jiangsu, China*
[2]*State Key Laboratory of Coal of Resources and Safe Ming, China University of Mining and Technology, Xuzhou 221116, Jiangsu, China*

Correspondence should be addressed to Jinhai Xu; jhxu118@126.com

Received 19 May 2021; Accepted 25 June 2021; Published 13 July 2021

Academic Editor: Junfei Zhang

To explore the influence of initial damage on the dynamic characteristics of rock mass, the Φ 50 mm split Hopkinson pressure bar (SHPB) test system was used, and the uniaxial impact compression tests on yellow sandstone specimens with different damage degrees were conducted, and then the variation law of mechanical properties of rock specimens with the initial damage was determined. The test results show that the dynamic stress-strain curve of rock specimens with initial damage can be roughly divided into compaction stage, elastic deformation stage, crack evolution stage, and strain-softening stage; the higher the initial damage degree of rock mass, the more significant the compaction stage. With the increase of the initial damage degree, the dynamic elastic modulus and peak stress of rock mass decrease gradually in a power number, while the peak strain of rock mass increases exponentially. With the increase of the initial damage degree, both the reflected energy ratio and the dissipated energy ratio decrease linearly, while the transmitted energy ratio increases linearly; the increasing rate of the transmitted energy ratio is greater than the decreasing rate of the reflected energy ratio.

1. Introduction

With the depletion of shallow coal resources, China's coal resources mining is gradually developing to the deep, and more deep roadway engineering will arise in future mining [1]. Before the excavation of roadways, there are many defects such as discontinuous nonconsecutive joints and fissures in the surrounding rock mass due to the geological tectonic movement. In the process of roadway excavation, the mechanical environment of the surrounding rock in the roadway is deteriorated due to unloading action [2]. As a result, a damaged area with poor mechanical performance parameters around the cavern is caused [3]. The roadway will be affected by long-term creep during service, resulting in cumulative damage to surrounding rock [4–6]. Although these unfavorable factors cannot directly cause rock failure, the formation of hidden cracks is greatly promoted. As mining depth increases, the stress level of the construction environment is increasing, and the occurrence frequency of induced dynamic disasters such as mine rock burst and coal and gas outburst (explosion) is also getting higher [7–9]. Therefore, the study of the dynamic characteristics of rock mass with the initial damage has important theoretical significance and engineering value, so as to reveal the dynamic instability mechanism of rock mass and maintain the stability of surrounding rock in the roadway [10, 11].

In previous studies, the static mechanical properties of rock mass with preexisting cracks have been mainly investigated by scholars. Pu et al. [12] and Xiao et al. [13], respectively, studied the failure modes of specimens with two preexisting consecutive cracks under uniaxial and triaxial loading conditions. Li et al. [14] carried out uniaxial compression tests on coal specimens with different inclination angles of preexisting crack [15]. The results show that the existence of cracks reduces the strength of coal; with the decrease of crack inclination, the peak strength is affected more and more obviously, showing a gradually decreasing trend. Liu et al. [16] performed the model test of rock mass

with preexisting joints and studied the strength and failure characteristics of jointed rock under the uniaxial compression. The results show that the failure mode and peak strength of jointed rock are closely related to the joint structure. Yang et al. [17, 18] conducted the conventional triaxial compression test on coarse marble with discontinuous preexisting cracks by the rock mechanics servo testing machine and explored the deformation and strength characteristics of coarse marble with discontinuous preexisting cracks under different confining pressures [19, 20]. On the basis of test results, the strength parameters of coarse marble with complete and discontinuous preexisting cracks were analyzed and compared by the strength criteria of the Coulomb and Hoek-Brown. Yang et al. [21] used simulation software of Particle Flow Code (PFC) to simulate the tensile strength and fracture propagation of the specimen with two discontinuous fractures. The results show that the tensile strength of rock specimens decreases with the increase of fracture length and rock bridge inclination; the wing fracture of the specimen is generally originated at the tip of the fracture, and the secondary fracture is generally originated at the boundary of the specimen. Besides, the inclination angle of the rock bridge and confining pressure have a great influence on the fracture expansion.

In the above research, rock specimens with preexisting cracks are mainly used. However, the rock cracks are irregular and disordered in real engineering. To this end, Huang [22] prepared coal specimens with different damage degrees by cyclic loading and unloading and carried out the triaxial compression tests and triaxial creep tests on coal specimens with different damage degrees [23, 24]. The test results show that, with the increase of initial damage degree, the compaction stage of coal specimens becomes shorter [25], while the strain-softening stage becomes longer; the "free-fall" failure (brittleness) at the peak value changes into "slow" failure (ductility); the more easily the dilatancy mechanism starts, the lower the deviatoric stress at the peak value is; with the increase of the initial damage degree, the total creep time is gradually shortened. Hou [26] prepared rock specimens with different damage degrees by applying different stress levels to the specimens and carried out creep tests under different confining pressures with the consideration of the effect of initial damage [27]. The study results show that the creep failure stress of rock with different initial damages is different; the larger the initial damage, the smaller the creep failure stress [28–31].

At present, static mechanical properties are mainly studied in the research on the initial damage of rock, and the specimens with preexisting cracks are mostly used as research objects. In this paper, rock specimens with different damage degrees were prepared by applying different freeze-thaw cycles to the specimens, and then the dynamic characteristics of rock specimens with different damage degrees were studied by using the SHPB test system. Finally, the influence of initial damage degree on dynamic characteristics and energy dissipation of rock specimens was analyzed.

2. Preparation of Rock Specimens with Different Initial Damage Degrees

2.1. Specimen Preparation. Yellow sandstone has relatively homogeneous grain structure and relatively uniform internal composition. To reduce the influence of rock dispersion and meet the requirements of rock impact dynamics test, yellow sandstone specimens (50 mm × 25 mm) with relatively uniform texture and good integrity were selected in this test. According to the standard for test methods of engineering rock mass (GB 50218-94), the two end faces of rock specimens were polished by double-end grinder to ensure the flatness of the two end faces ≤0.5 mm and the parallelism of the two end faces ≤0.02 mm. After processing, the specimen surface was smooth without damage, satisfying the test accuracy requirements for rock specimens used in the test. Table 1 shows the basic physical and mechanical parameters of a standard specimen with a size of 50 × 100 mm under the static load.

2.2. Experimental Equipment. In this test, the longitudinal wave velocity of the specimen was measured by the HC-U81 nonmetallic ultrasonic detector purchased from Hichance high-tech, as shown in Figure 1(a). The saturated water specimen was prepared by the vacuum saturated container of the Shanghai geotechnical highway instrument company, as shown in Figure 1(b). The freeze-thaw cycle test of the specimen was carried out by JC-ZDR-5 automatic low-temperature freeze-thaw tester, as shown in Figure 1(c). The specimen was dried by DHG-9076 electric constant-temperature drying oven, as shown in Figure 1(d).

2.3. Initial Damage Test of Structural Rock under the Low-Temperature Freeze-Thaw Cycles. In this experiment, yellow sandstone specimens were subjected to different numbers of low-temperature freeze-thaw cycles to obtain different initial damage degrees (D_w).

Firstly, the longitudinal wave velocity of the specimen was tested by the ultrasonic detector. To reduce the influence of the specimen dispersion on experimental results, the specimen with a larger deviation of the wave velocity was removed, and the specimens with the same wave velocity value were selected for the subsequent experiment.

According to relevant regulations of water absorption test in the code for rock tests of hydroelectric and water conservancy engineering (DL/T5368-2007), specimens were immersed in the vacuum saturated container, and the air was pumped into a vacuum, then the saturated specimens were prepared. Subsequently, the saturated specimens were put into the low-temperature freeze-thaw testing machine at a freeze-thaw temperature of −20°C for 12 hours; and then the temperature was adjusted to 20°C for 12 hours to completely melt the ice inside the yellow sandstone. This process was a whole freeze-thaw cycle. According to the specimen number, the yellow sandstone was subjected to 5, 10, 20, and 30 freeze-thaw cycles in the low-temperature freeze-thaw chamber. Figure 2 shows some yellow sandstone specimens after the freeze-thaw cycles. Finally, the yellow sandstone

Table 1: Physical and mechanical parameters of rock specimen.

Mass (g)	Density (kg·m^{-3})	Compressive strength (MPa)	Peak strain (10^{-2})	Elastic modulus GPa	Poisson ratio
493.92	2287	51.46	1.167	5.76	0.22

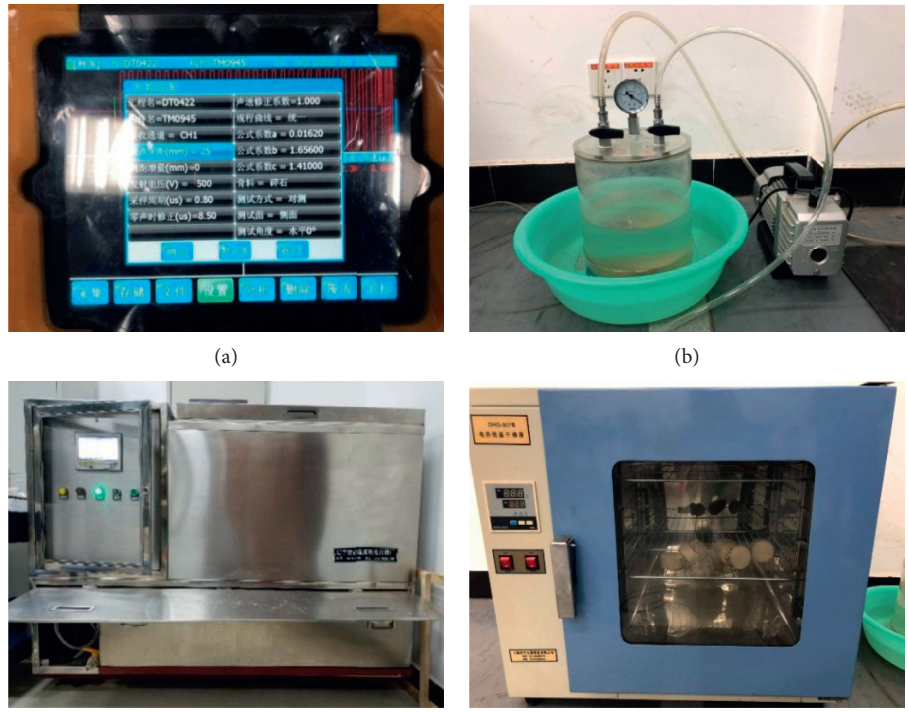

(a) (b) (c) (d)

Figure 1: Test equipment. (a) Nonmetal ultrasonic detector. (b) Vacuum saturated container. (c) Low-temperature freeze-thaw tester. (d) Electric constant-temperature drying oven.

Figure 2: Some yellow sandstone specimens after freeze-thaw cycles.

specimens after low-temperature freeze-thaw cycles were placed in the thermostatic drying oven at 105°. After 24 hours, the specimens were taken out from the drying oven.

2.4. Damage Degree of Rock. During the freeze-thaw cycles of rock, the water in the saturated rock specimen is always circulating between the solid phase and the liquid phase. Due to the volume expansion of the water in the solid phase, the pore pressure will be formed between the micropores in the rock, resulting in the generation and expansion of the microcracks in the rock. The generation and expansion of the microcracks not only affect the mechanical properties of the rock but also change the elastic wave propagation velocity in the rock medium. Therefore, the damage variable reflecting the deterioration of rock mechanical properties is correlated to the sound velocity, and the rock response caused by damage must be reflected in the change of sound wave velocity in rock. By measuring the change of wave velocity before and after damage, the comprehensive damage degree of rock is analyzed, which can be expressed as

$$D_w = 1 - \left(\frac{V_0}{V}\right)^2, \tag{1}$$

where V_0 is the longitudinal wave velocity of rock without damage and V is the longitudinal wave velocity after damage.

The longitudinal wave velocity of specimens before and after freeze-thaw cycles was measured by the ultrasonic detector, and the damage degree D_w of each specimen was calculated. Table 2 shows the damage degree of specimens, and Figure 3 shows the influence of freeze-thaw cycles on damage degree.

Table 2 and Figure 3 show the influence of the number n of freeze-thaw cycles on the damage degree D_w. With the increase of the number of freeze-thaw cycles, the damage degree D_w of

Table 2: Damage degree of yellow sandstone under different freeze-thaw cycles.

No.	Freeze-thaw cycles n	V_0 (km/s)	V (km/s)	D_w	Average
X0-1		2.688	2.688	0	
X0-2	0	2.688	2.688	0	0
X0-3		2.688	2.688	0	
X5-1		2.688	1.974	0.461	
X5-2	5	2.688	1.956	0.470	0.465
X5-3		2.688	1.968	0.463	
X10-1		2.688	1.613	0.640	
X10-2	10	2.688	1.588	0.650	0.643
X10-3		2.688	1.632	0.631	
X20-1		2.688	1.341	0.736	
X20-2	20	2.688	1.352	0.747	0.742
X20-3		2.688	1.347	0.741	
X30-1		2.688	1.111	0.829	
X30-2	30	2.688	1.134	0.822	0.823
X30-3		2.688	1.143	0.819	

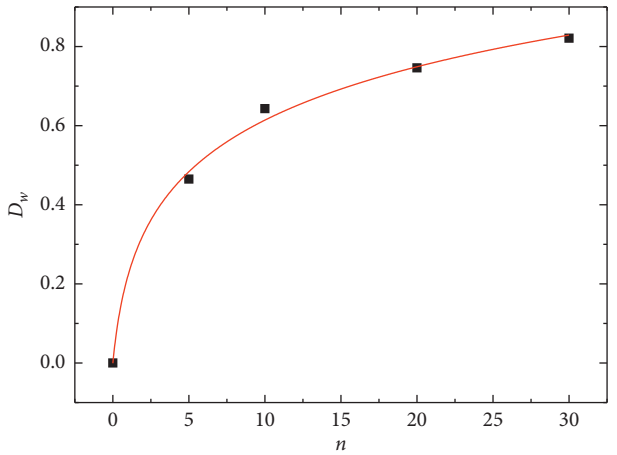

Figure 3: Effect of the number n of freeze-thaw cycles on damage degree D_w.

the specimen becomes larger and larger. When the number of freeze-thaw cycles exceeds 15, the increasing trend of D_w slows down and presents a logarithmic increase. Since there is an upper limit for the volume expansion of a certain volume of water during solidification, the damage to the yellow sandstone specimen at −20°C gradually slows down. When the damage reaches a certain degree, the increase of cycle number reduces the damage rate of yellow sandstone specimen. According to the change characteristics of damage degree D_w with the number of freeze-thaw cycles n, the function formula is obtained by curve fitting method as follows:

$$D_w = 0.202 \ln(n + 0.498) + 0.140, \quad R^2 = 0.9941. \tag{2}$$

3. Rock Dynamics Test Equipment and Methods

3.1. Experimental Equipment. The Φ 50 mm SHPB test system of State Key Laboratory of Geomechanics and Deep Underground Engineering of China University of Mining and Technology was adopted in this test, as shown in Figure 4(a). The whole system was composed of five parts: loading drive system, pressure bar system, energy absorption system, signal acquisition system, and signal processing system. As shown in Figure 4(b), a high-speed camera was used to record the whole failure process of the specimen under uniaxial compression impact load.

3.2. Experimental Methods. Yellow sandstone specimens with initial damage degree D_w of 0, 0.465, 0.643, 0.742, and 0.823 after freeze-thaw cycle were used, and 3 specimens were taken for each damage degree. The impact load of 0.3 MPa was applied to the input air pressure of the system, and the specimens were compressed to the failure. The test data were processed by three-wave method.

4. Test Results and Discussion

4.1. Characteristics of Stress-Strain Curves. Figure 5 shows the whole process stress-strain curves of yellow sandstone specimens with different damage degrees. The whole process of specimen failure is recorded by a high-speed camera, as shown in Figure 6. It can be seen that the stress-strain curves of rocks with different damage degrees under the high strain rate can be roughly divided into the following stages.

(1) Compaction stage ($d^2\sigma/d\varepsilon^2 > 0$): In this stage, the stress-strain curve shows a concave shape. The higher the initial damage, the longer the compaction stage. The higher the initial damage, the more the internal microcracks and micropores inside the specimen. Under the action of axial stress, the internal microcracks are gradually closed, and the micropores and other defects are gradually shrunk. Therefore, the higher the damage degree, the longer the compaction stage.

(2) Elastic deformation stage ($d^2\sigma/d\varepsilon^2 = 0$): As shown in Figure 6(a), at this stage, the microcracks and micropores inside the rock are basically closed and in a stable state. The elastic energy is continuously accumulated, which is not enough to promote the crack expansion or new crack generation inside the rock specimens. Moreover, the higher the initial damage, the shorter the elastic deformation stage. The relationship between stress and strain is linear at this stage, and the slope of the curve is basically unchanged. Therefore, the slope of the curve at this stage can be used as the dynamic elastic modulus of rock.

(3) Crack evolution stage ($d^2\sigma/d\varepsilon^2 < 0$): In this stage, the slope of the stress-strain curve decreases and the curve is convex. The stress acting on the rock specimen increases continuously, leading to the expansion of initial microcracks of the rock specimen and the generation of new cracks, as shown in Figure 6(b). As a result, the mechanical properties of the rock specimen are reduced.

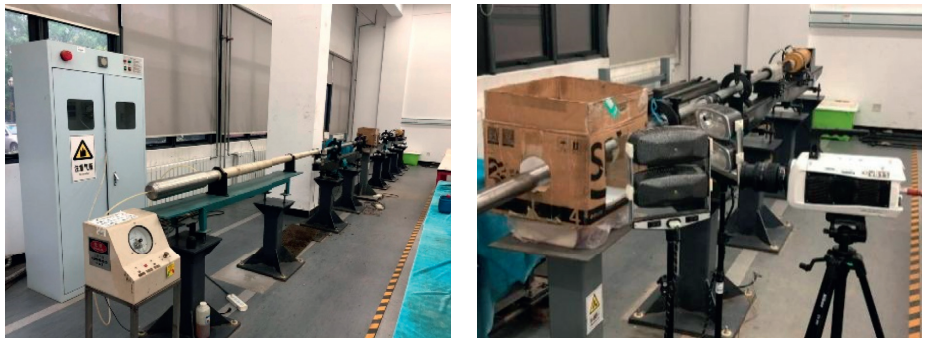

(a) (b)

Figure 4: Dynamic test equipment. (a) SHPB test system. (b) High-speed camera.

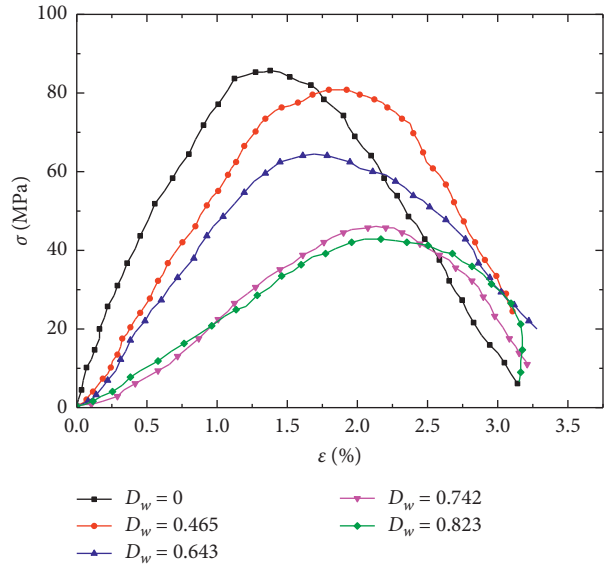

Figure 5: Stress-strain curves of sandstone with different initial damage degrees.

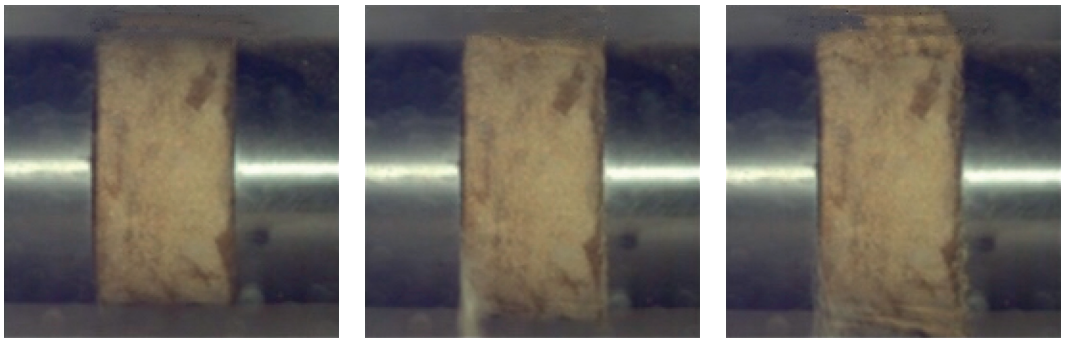

Compaction and elastic deformation stage (a) Crack evolution stage (b) Specimen failure (c)

Figure 6: Loading process of specimen. (a) Compaction and elastic deformation stage. (b) Crack evolution stage. (c) Specimen failure.

(4) Strain-softening stage ($d\sigma/d\varepsilon < 0$): In this stage, the curve shows a downward trend, and the internal microcracks of the rock specimen develop and penetrate the specimen, as shown in Figure 6(c). The specimen is basically completely broken and loses its bearing capacity.

4.2. Variation Law of Dynamic Characteristic Parameters. According to the whole stress-strain curves of yellow sandstone with different damage degrees, the variation laws of dynamic elastic modulus E_d, peak stress σ_d, and peak strain ε_d of sandstone with initial damage degree D_w are obtained, as shown in Table 3.

4.2.1. Variation Characteristics of Dynamic Elastic Modulus E_d. Dynamic elastic modulus E_d is an important index of dynamic mechanical properties of rock, which can represent the resistance of rock to elastic deformation under a high strain rate. Figure 7 shows the variation curve of dynamic elastic modulus E_d of sandstone with initial damage degree D_w. With the increase of the initial damage degree D_w of the yellow sandstone specimen, the elastic modulus E_d decreases gradually in a power number. When the initial damage degree D_w increases from 0 to 0.465, the elastic modulus E_d decreases slowly from 59.17 GPa to 54.42 GPa, with a decrease of 8.03%. When the initial damage degree D_w increases from 0.465 to 0.823, the elastic modulus E_d decreases rapidly from 54.42 GPa to 27.15 GPa, with a decrease of 50.66%. The higher the initial damage degree of sandstone specimens, the more the internal structure defects such as pore cracks, the worse the resistance to deformation, and the lower the elastic modulus. By using the curve fitting method, the relationship between the dynamic elastic modulus E_d and the sandstone with initial damage degree D_w is obtained as follows:

$$\begin{aligned} E_d &= -50.065D_w^2 + 62.260, \\ R^2 &= 0.9246. \end{aligned} \tag{3}$$

4.2.2. Variation Characteristics of Dynamic Peak Stress σ_d. The dynamic peak stress represents the ultimate bearing capacity of rock at the high strain rate. Figure 8 shows the variation curve of dynamic peak stress σ_d of sandstone with initial damage degree D_w. It can be seen that, with the increase of initial damage degree D_w, the peak stress σ_d decreases gradually in a power number. There is an obvious turning point in the curve. When the initial damage D_w increases from 0 to 0.465, the peak stress σ_d decreases slowly, from 90.53 MPa to 82.62 MPa, with a decrease of 8.74%. When the initial damage D_w increases from 0.465 to 0.742, the peak stress σ_d of sandstone specimen decreases rapidly from 82.62 MPa to 44.41 MPa, with a decrease of 46.25%. When the initial damage degree D_w increases from 0.742 to 0.823, the peak stress σ_d also decreases, and the decline amplitude decreases gradually. According to the variation curve of sandstone dynamic peak stress σ_d with initial damage degree D_w, its relation can be obtained as

$$\begin{aligned} \sigma_d &= -80.780D_w^2 + 94.699, \\ R^2 &= 0.9348. \end{aligned} \tag{4}$$

4.2.3. Variation Characteristics of Dynamic Peak Strain ε_d. Dynamic peak strain represents the ultimate deformation degree of rock at peak stress under the high strain rate. Figure 9 shows the relationship between the peak strain ε_d of sandstone and the initial damage degree D_w. With the increase of the initial damage degree D_w sandstone specimen, the peak strain ε_d shows an upward trend, and the whole process can be roughly divided into two stages. In the first stage, the initial damage degree D_w increases from 0 to 0.465, and the peak strain ε_d increases from 0.0118 to 0.0127, with an increase of 7.63%. In the second stage, the initial damage degree D_w increases from 0.465 to 0.823, and the peak strain ε_d increases from 0.0127 to 0.0193 in a straight line, with an increase of 51.97%. Besides, the increasing amplitude is much higher than that in the previous stage. Using the curve fitting method, the relationship between the dynamic peak strain ε_d and the initial damage degree D_w is obtained as follows:

$$\begin{aligned} \varepsilon_d &= 1.105 + 0.050e^{3.440D_w}, \\ R^2 &= 0.9374. \end{aligned} \tag{5}$$

The higher the initial damage is, the larger the internal structure of rock specimen is damaged. Under the compression, the pores and cracks expand rapidly, forming a large number of cracks. Macroscopically, the rock specimen has a larger compression deformation, which leads to the increase of peak strain.

5. Energy Dissipation Law of Rock with Initial Damage

The failure process of rock is accompanied by energy absorption and dissipation. Therefore, the study of energy dissipation law can effectively reveal the dynamic failure characteristics and failure law of rock mass.

5.1. Calculation Method of Energy Dissipation. The SHPB test device was used to collect the incident wave, reflected wave, and transmitted wave signals during the test. The incident energy, reflected energy, and transmitted energy can be obtained by the following:

$$\begin{cases} W_I = E_0 C_0 A_0 \int_0^t \varepsilon_I^2(t)\mathrm{d}t, \\ W_R = E_0 C_0 A_0 \int_0^t \varepsilon_R^2(t)\mathrm{d}t, \\ W_T = E_0 C_0 A_0 \int_0^t \varepsilon_T^2(t)\mathrm{d}t, \end{cases} \tag{6}$$

where W_I, W_R, and W_T are the incident energy, reflected energy, and transmitted energy, respectively, C_0 is the propagation velocity of stress wave in the rod, A_0 and E_0

Table 3: Dynamic mechanical parameters of sandstone with different damage degrees.

No.	E_d (GPa)		σ_d (MPa)		ε_d (%)	
	Single specimen	Average	Single specimen	Average	Single specimen	Average
X0-1	57.68		93.57		1.09	
X0-2	61.65	59.17	86.48	90.53	1.18	1.18
X0-3	58.17		91.53		1.28	
X5-1	52.78		84.94		1.21	
X5-2	57.17	54.42	79.84	82.62	1.34	1.27
X5-3	53.31		83.09		1.27	
X10-1	43.31		63.75		1.68	
X10-2	46.76	45.57	66.01	65.38	1.56	1.63
X10-3	46.63		66.38		1.64	
X20-1	29.03		44.87		1.76	
X20-2	35.49	31.95	43.22	44.41	1.71	1.76
X20-3	31.32		45.15		1.82	
X30-1	28.49		43.89		1.94	
X30-2	25.34	27.15	41.94	40.50	1.86	1.93
X30-3	27.63		35.67		1.98	

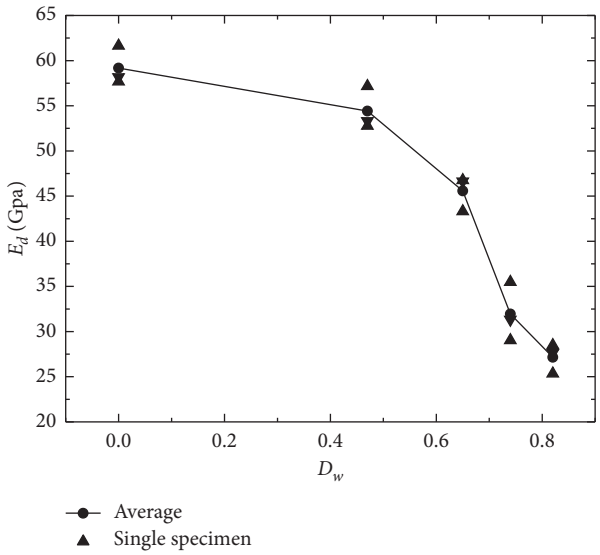

Figure 7: Variation curve of dynamic elastic modulus E_d changing with the initial damage degree D_w.

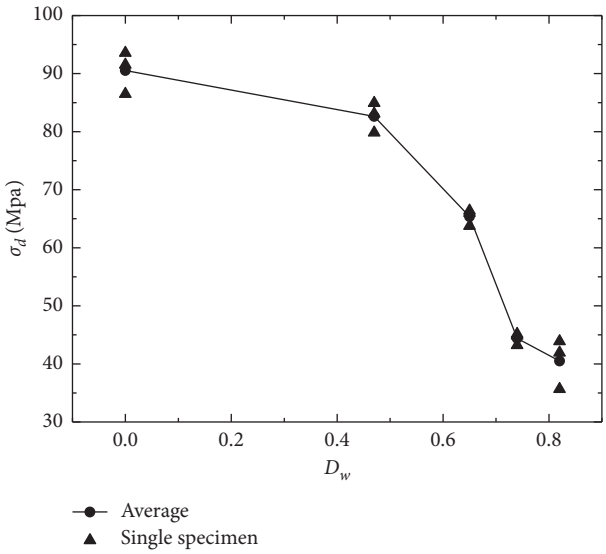

Figure 8: Variation curves of dynamic peak stress σ_d with initial damage degree D_w.

are the diameter and elastic modulus of the rod, respectively, and ε_I, ε_R, and ε_T are the collected incident wave, reflected wave, and transmitted wave signals, respectively.

According to the SHPB test principle, the dissipated energy in the system is

$$W_L = W_I - (W_R + W_T). \quad (7)$$

5.2. Effect of Initial Damage on Dynamic Energy Dissipation Characteristics of Sandstone. According to the energy calculation method, the energy values of sandstone specimens with different initial damage degrees during the failure process are obtained. The percentages of reflected energy W_R, transmitted energy W_T, and dissipated energy W_L to the incident energy W_I are defined as R_R, R_T, and R_L, respectively, as shown in Table 4. The variation curve of energy ratios with initial damage degree D_w is shown in Figure 10.

As shown in Table 4, under the same strain rate, the incident energy is about 114 J. Considering the small differences, the energy ratios R_R, R_T, and R_L are taken as parameters. Then the variation law of energy dissipation with the initial damage degree D_w of rock is analyzed.

As shown in Figure 10, with the change of initial damage degree D_w of the rock specimen, the energy ratios show significant changes. With the increase of initial damage degree D_w, the reflected energy ratio R_R decreases linearly, and the reflected energy ratio R_R at the damage degree of 0 is 1.12 times that at damage degree of 0.823. The variation law of transmitted energy ratio R_T is different. With the increase of initial damage degree D_w, the transmitted energy ratio R_T increases linearly; the growth rate of R_T is greater than the

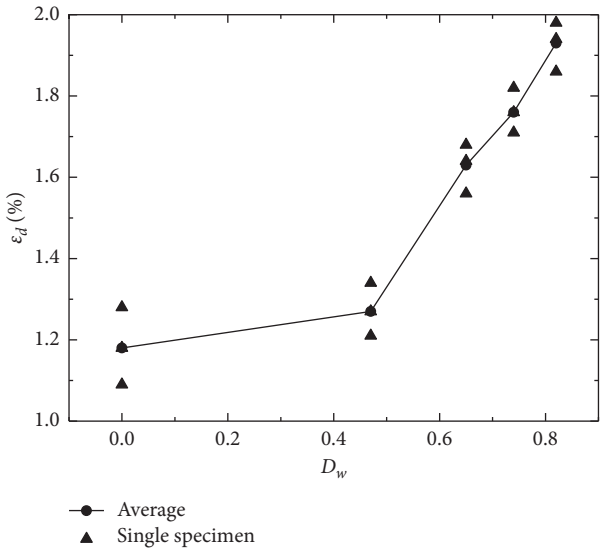

Figure 9: Variation curves of dynamic peak strain ε_d with the initial damage degree D_w.

Table 4: Energy values of specimens during failure.

No.	X0	X5	X10	X20	X30
W_I (J)	114.74	113.60	114.64	115.11	113.84
W_R (J)	62.83	59.05	57.57	57.35	55.49
R_R (%)	54.76	51.98	50.22	49.82	48.74
W_J (J)	21.53	30.17	32.94	36.93	38.86
R_T (%)	18.76	26.56	28.73	32.09	34.14
W_L (J)	30.38	24.38	24.13	20.83	19.49
R_L (%)	26.48	21.46	21.05	18.10	17.12

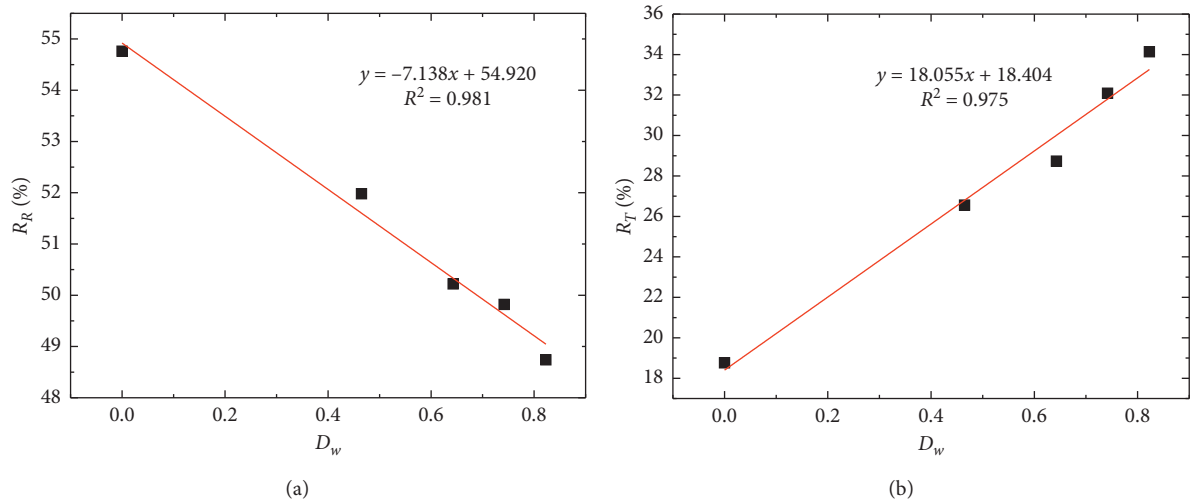

(a) (b)

Figure 10: Continued.

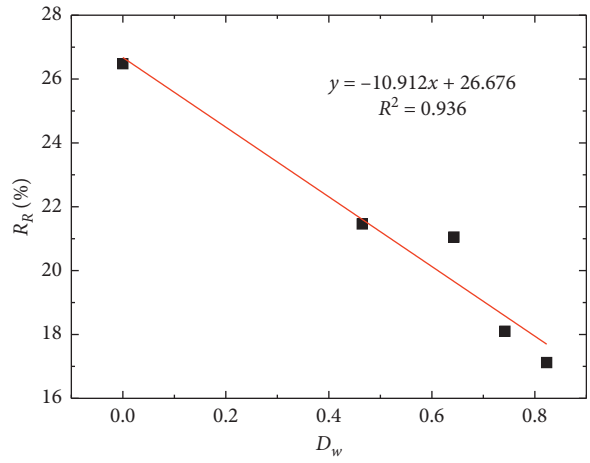

(c)

Figure 10: Variation of different energy ratios with the initial damage degree D_w. (a) Reflected energy ratio R_R changing with D_w. (b) Transmitted energy ratio R_T changing with D_w. (c) Dissipated energy ratio R_L changing with D_w.

decreasing rate of the reflected energy ratio R_R. The transmitted energy ratio R_T at damage degree of 0.823 is 1.82 times that at damage degree of 0. The variation law of the dissipated energy ratio R_L is similar to that of the reflected energy ratio R_R. With the increase of initial damage degree D_w, R_L also decreases linearly. The dissipated energy ratio R_L at the damage degree of 0 is 1.55 times that at the damage degree of 0.823.

With the increase of the initial damage degree D_w, the energy dissipation capacity of the specimen decreases gradually. From the perspective of energy dissipation, when the initial damage degree of rock specimens is low, the internal cracks of the specimen are less, and more energy is needed to promote the propagation of microcracks and the generation of new cracks, thus leading to rock fracture. This energy dissipation law reflects the essential characteristics of rock deformation and failure.

6. Conclusions

In this paper, specimens with different initial damage degrees are obtained by freeze-thaw cycles, and the mechanical properties of sandstones with initial damage from 0 to 0.823 are studied on the SHPB test system. The main conclusions are as follows:

(1) With the increasing number of freeze-thaw cycles, the damage degree D_w of the specimen increases; when the number of freeze-thaw cycles exceeds 15, the increasing trend of D_w slows down and presents a logarithmic increase.

(2) Stress-strain curve of specimens with the initial damage can be roughly divided into compaction stage, elastic deformation stage, crack evolution stage, and strain-softening stage. The higher the initial damage, the longer the compaction stage.

(3) With the increase of initial damage degree D_w, the dynamic elastic modulus and peak stress of the specimen decrease gradually in a power number. When the initial damage degree D_w increases from 0 to 0, the elastic modulus and peak stress decrease by 8.03% and 8.74%. When the initial damage degree D_w increases from 0.465 to 0.823, the elastic modulus and peak stress all decrease by about 50%.

(4) With the increase of initial damage degree D_w of sandstone specimens, the peak strain increases exponentially. When the initial damage degree D_w increases from 0 to 0.465, the peak strain increases by 7.63%; when the initial damage degree D_w increases from 0.465 to 0.823, the peak strain increases by 51.97%.

(5) The energy ratio is taken as a parameter to analyze different energy values changing with the initial damage degree. With the increase of initial damage degree D_w, the reflected energy ratio R_R and dissipated energy ratio R_L decrease linearly, while the transmitted energy ratio R_T increases linearly; the growth rate of R_T is greater than the decreasing rate of the reflected energy ratio R_R.

Data Availability

The data used to support the findings of this study are included within the article.

Conflicts of Interest

The authors declare that they have no conflicts of interest.

Acknowledgments

This research was funded by National Natural Science Foundation (52074240) and independent research project of State Key Laboratory of Coal Resources and Safe Mining, CUMT (SKLCRSM2020X05).

References

[1] H. P. Xie, F. Gao, and Y. Ju, "Research and exploration of deep rock mechanics," *Chinese Journal of Rock Mechanics and Engineering*, vol. 34, no. 11, pp. 2161–2178, 2015.

[2] D. Ma, J. J. Wang, X. Cai et al., "Effects of height/diameter ratio on failure and damage properties of granite under coupled bending and splitting deformation," *Engineering Fracture Mechanics*, vol. 220, Article ID 106640, 2019.

[3] Z. Huang, S. Li, K. Zhao, Y. Wu, W. Zeng, and H. Xu, "Estimating the hydraulic conductivity of deep fractured rock strata from high-pressure injection tests," *Mine Water and the Environment*, vol. 39, no. 1, pp. 112–120, 2020.

[4] Y. Kang, X. H. Li, and C. H. Yang, "Research on numerical tests on damaged-failure mode of surrounding rock in deep buried tunnel," *Chinese Journal of Rock Mechanics and Engineering*, vol. 26, no. S1, p. 3578, 2007.

[5] D. Ma, H. Duan, Q. Zhang et al., "A numerical gas fracturing model of coupled thermal, flowing and mechanical effects," *Computers, Materials & Continua*, vol. 65, no. 3, pp. 2123–2141, 2020.

[6] Y. S. Wang, L. J. Ma, and X. Y. Liu, "Development in research on creep and fatigue damage of rock," *Industrial Construction*, vol. 46, no. 4, pp. 120–127, 2016.

[7] H. Xie, H. Zhou, D. Xue et al., "Research and consideration on deep coal mining and critical mining depth," *Journal of China Coal Society*, vol. 37, no. 4, pp. 535–542, 2012.

[8] A. Teymen and E. C. Mengüç, "Comparative evaluation of different statistical tools for the prediction of uniaxial compressive strength of rocks," *International Journal of Mining Science and Technology*, vol. 30, no. 6, pp. 785–797, 2020.

[9] D. Ma, H. Duan, J. Liu, X. Li, and Z. Zhou, "The role of gangue on the mitigation of mining-induced hazards and environmental pollution: an experimental investigation," *The Science of the Total Environment*, vol. 664, pp. 436–448, 2019.

[10] Z. Huang, Z. Jiang, S. Zhu, X. Wu, L. Yang, and Y. Guan, "Influence of structure and water pressure on the hydraulic conductivity of the rock mass around underground excavations," *Engineering Geology*, vol. 202, pp. 74–84, 2016.

[11] L. Y. Wu, H. B. Bai, and D. Ma, "Prediction and prevention of water inrush hazards from bed separation space," *Mine Water and the Environment*, 2021.

[12] C. Pu, P. Cao, Y. Yi et al., "Fracture for rock-like materials with two transfixion fissures under uniaxial compression," *Journal of Central South University*, vol. 43, no. 7, pp. 2708–2716, 2012.

[13] T. Xiao, X. Li, and S. Jia, "Experimental study on failure characteristics of rock specimens with two discontinuous through pre-existing cracks under triaxial compression," *Chinese Journal of Rock Mechanics and Engineering*, vol. 34, no. 12, pp. 2455–2462, 2015.

[14] D. Li, E. Wang, N. Li et al., "Research on coal characteristic of macro-crack dip angle under uniaxial compression," *Chinese Journal of Rock Mechanics and Engineering*, no. S1, pp. 93–100, 2017.

[15] D. Ma, H. Duan, W. Liu, X. Ma, and M. Tao, "Water-sediment two-phase flow inrush hazard in rock fractures of overburden strata during coal mining," *Mine Water and the Environment*, vol. 39, no. 2, pp. 308–319, 2020.

[16] H. Liu, Y. Huang, K. Li et al., "Test study of strength and failure mode of pre-existing jointed rock mass," *Rock and Soil Mechanics*, no. 5, pp. 1235–1241, 2013.

[17] S. Yang, S. Wen, and L. Li, "Experimental study on deformation and strength properties of coarse marble with discontinuous pre-existing cracks under different confining pressures," *Chinese Journal of Rock Mechanics and Engineering*, vol. 26, no. 8, pp. 1572–1587, 2006.

[18] S. Yang, Y. Jiang, and S. Wen, "Study on strength parameters of coarse marble with two pre-existing cracks," *Engineering Mechanics*, vol. 25, no. 12, pp. 127–134, 2008.

[19] D. Ma, H. Y. Duan, X. B. Li, Z. H. Li, Z. L. Zhou, and T. B. Li, "Effects of seepage-induced erosion on nonlinear hydraulic properties of broken red sandstones," *Tunnelling and Underground Space Technology*, vol. 91, Article ID 102993, 2019.

[20] Z. Huang, Z. Jiang, S. Zhu, Z. Qian, and D. Cao, "Characterizing the hydraulic conductivity of rock formations between deep coal and aquifers using injection tests," *International Journal of Rock Mechanics and Mining Sciences*, vol. 71, pp. 12–18, 2014.

[21] S. Yang, Y. Huang, and X. Liu, "Particle flow analysis on tensile strength and crack coalescence behavior of brittle rock containing two pre-existing fissures," *Journal of China University of Mining and Technology*, vol. 43, no. 2, pp. 220–226, 2014.

[22] P. Huang, *Study on the Creep Damage Mechanism of Coal Petrography and Gob-Side Coal Pillar Stability*, China University of Mining & Technology, Xuzhou, China, 2018.

[23] Q. Zhang, D. Ma, Y. Wu, and F. Meng, "Coupled thermal−gas−mechanical (TGM) model of tight sandstone gas wells," *Journal of Geophysics and Engineering*, vol. 15, no. 4, pp. 1743–1752, 2018.

[24] Y. L. Huang, J. M. Li, D. Ma, H. D. Gao, Y. C. Guo, and S. Y. Ouyang, "Triaxial compression behaviour of gangue solid wastes under effects of particle size and confining pressure," *The Science of the Total Environment*, vol. 693, Article ID 133607, 2019.

[25] D. Ma, J. X. Zhang, H. Y. Duan et al., "Reutilization of gangue wastes in underground backfilling mining: overburden aquifer protection," *Chemosphere*, vol. 264, no. 1, Article ID 128400, 2021.

[26] R. B. Hou, *Effects of Initial Damage on Time-Dependent Behavior of Soft Rock Roadway and Control Countermeasure*, China University of Mining & Technology, Xuzhou, China, 2018.

[27] M. Ghorbani, K. Shahriar, M. Sharifzadeh, and R. Masoudi, "A critical review on the developments of rock support systems in high stress ground conditions," *International Journal of Mining Science and Technology*, vol. 30, no. 5, pp. 555–572, 2020.

[28] T. Xu, P. G. Ranjith, P. L. P. Wasantha, J. Zhao, C. A. Tang, and W. C. Zhu, "Influence of the geometry of partially-spanning joints on mechanical properties of rock in uniaxial compression," *Engineering Geology*, vol. 167, pp. 134–147, 2013.

[29] G.-L. Zhou, T. Xu, M. J. Heap et al., "A three-dimensional numerical meso-approach to modeling time-independent deformation and fracturing of brittle rocks," *Computers and Geotechnics*, vol. 117, Article ID 103274, 2020.

[30] T.-F. Fu, T. Xu, M. J. Heap, P. G. Meredith, and T. M. Mitchell, "Mesoscopic time-dependent behavior of rocks based on three-dimensional discrete element grain-based model," *Computers and Geotechnics*, vol. 121, Article ID 103472, 2020.

[31] T. Xu, T.-F. Fu, M. J. Heap, P. G. Meredith, T. M. Mitchell, and P. Baud, "Mesoscopic damage and fracturing of heterogeneous brittle rocks based on three-dimensional polycrystalline discrete element method," *Rock Mechanics and Rock Engineering*, vol. 53, no. 12, pp. 5389–5409, 2020.